Revisiting Subglacial Hydrology as an Origin for Mars' Valley Networks

J. J. Buffo[1], **L. Ojha**[2], **C. R. Meyer**[1], **K. L. Ferrier**[3], **and M. C. Palucis**[4]
1 – Thayer School of Engineering, Dartmouth College, Hanover, NH, USA
2 – Department of Earth and Planetary Sciences, Rutgers, Piscataway, NJ, USA
3 – Department of Geoscience, University of Wisconsin, Madison, WI, USA
4 – Department of Earth Sciences, Dartmouth College, Hanover, NH, USA

Abstract

Although the nature of the early Martian climate is a matter of considerable debate, the presence of valley networks (VN) provides unambiguous evidence for the presence of liquid water on Mars' surface. A subaerial fluvial origin of VN is at odds with the expected phase instability of near-surface water in the cold, dry Late Noachian climate. Furthermore, many observed geomorphometric properties of VN are inconsistent with surface water flow. Conversely, subglacial channels exhibit many of these characteristics and could have persisted beneath ice sheets even in a cold climate. Here we model basal melting beneath a Late Noachian Icy Highlands ice sheet and map subglacial hydrological flow paths to investigate the distribution and geomorphometry of subglacial channels. We show that subglacial processes produce enough melt water to carve Mars' VN; that predicted channel distribution is consistent with observations; and corroborate geomorphometric measurements of VN consistent with subglacial formation mechanisms. We suggest that subglacial hydrology may have played a key role in the surface modification of Mars.

Plain Language Summary

Thousands of valley networks on Mars appear to have been carved by flowing water, and exhibit branching characteristics akin to river networks on Earth. Their origins, however, remain enigmatic for two primary reasons. First, ancient Mars was potentially cold, dry, and unable to support liquid water on its surface. Second, many physical characteristics of the valleys are inconsistent with features formed by precipitation and runoff. On Earth, water flowing beneath ice sheets produces channels with similar characteristics to Mars' valley networks. Here we model the deposition and evolution of Martian ice sheets and show that melting at the ice sheet base is likely even under cold and dry surface conditions. The volume, regional distribution, and flow patterns of melt are consistent with the volume and dynamics needed to carve the observed valley networks. A subglacial origin for Mars' valley networks accounts for their formation in a cold, dry climate and produces valley characteristics that match observations. In addition to improving our knowledge of the role that ice sheets play in shaping Mars' surface, water rich regions at the base of ice sheets could be habitable environments.

Keywords

Mars, Valley Networks, Subglacial Channels, Subglacial Hydrology

1. Introduction

A puzzling class of geomorphic features on Mars is the widespread valley networks (VN) carved into the planet's surface [*Carr and Malin*, 2000; *Hynek et al.*, 2010; *Luo and Stepinski*, 2009; *Rossman III et al.*, 2008]. Concentrated in the southern mid-latitudes (Supplementary Figure S1), these features were initially assumed to be the result of surface water flow, exhibiting branching channel structures similar to those of terrestrial river systems (e.g. [*Milton*, 1973; *Seybold et al.*, 2018]). Upon further observation, however, a number of VN properties are inconsistent with precipitation or groundwater driven formation mechanisms [*Carr and Malin*, 2000; *Gulick*, 2001; *Pieri*, 1980]: U-shaped or rectangular valley cross sections; deep valley incision; uniform valley width over long distances; a dearth of small scale (<100 m wide) valleys – although this could be due to erosive processes [*Hynek et al.*, 2010]; and the need for substantial surface runoff and precipitative/aquifer recharge capable of transporting the large volume of eroded sediment [*Carr and Malin*, 2000; *Grau Galofre et al.*, 2020]. Additionally, numerous (though not all [*Haberle et al.*, 2019]) climate models support the idea that the early history of Mars was dominated by cold, dry conditions not conducive to a hydrological cycle capable of forming the VN (e.g. [*Haberle*, 1998; *Wordsworth et al.*, 2013; *Wordsworth*, 2016]). Any proposed formation scenario for Mars' VN should be consistent with these observations and model predictions.

A particularly promising solution is the possibility that glacial processes could have played a key role in sculpting the VN we see today. While this is not a new proposition (e.g., [*Kargel and Strom*, 1992; *Lucchitta et al.*, 1981]) our understanding of terrestrial subglacial dynamics is evolving, providing new insights when applied to the Martian environment [*Head and Marchant*, 2014; *Hewitt*, 2011; *Werder et al.*, 2013]. A promising feature of the glacially driven VN formation mechanism theory is that it addresses several of the characteristics of VN that are unresolved by precipitation/groundwater driven formation processes (Supplementary Figure S1). Glacial valleys typically exhibit U-shaped cross-sectional profiles, as opposed to the V-shaped profiles of fluvially carved valleys [*Carr and Head III*, 2003; *Carr and Malin*, 2000; *Grau Galofre et al.*, 2020]. Similarly, deep valleys with constant widths are a hallmark of glacially carved valleys [*Grau Galofre and Jellinek*, 2017; *Grau Galofre et al.*, 2018]. Distributed, rather than channelized, flow beneath an ice sheet could explain the lack of small-scale (< 100 m) channels on the Martian surface. For example, under thick terrestrial ice deposits, sheet-like flow in the porous sediment dominates until the water reaches larger low-pressure drainage channels [*Hewitt*, 2011; *Meyer et al.*, 2016; *Sommers et al.*, 2018; *Werder et al.*, 2013]. Furthermore, the insulating properties of an ice sheet can facilitate geothermal heat driven basal melt even under cold, dry climate conditions [*Fastook and Head*, 2015; *Ojha et al.*, *2020*]. Subglacial drainage coupled with sublimation and snow deposition can provide a hydrologic/cryologic cycle that is able to recharge an ice sheet and thus provide a mechanism for continuous erosion. Lastly, the presence of VN on younger, high-elevation terrain associated with volcanic features (e.g. Alba, Olympus, Elysium, and Tharsis Mons) suggests ice/snow melting caused by basal heating, in this case from magmatic sources, could have been a recurring erosive process throughout Mars' history [*Butcher et al.*, 2017; *Gallagher and Balme*, 2015; *Scanlon et al.*, 2015].

Previous studies have shown that basal melting is possible beneath ice deposits under historic Martian climate conditions [*Carr and Head III*, 2003; *Fastook and Head*, 2015; *Ojha et al.*, *2020*]. Additionally, numerous studies have identified morphological features across Mars' surface that are consistent with widespread glaciation (e.g. [*Carr and Head III*, 2003; *Carr and Malin*, 2000; *Grau Galofre et al.*, 2020; *Kargel et al.*, 1995]). Recently, *Grau Galofre et al.* [2020]

conducted a detailed investigation of VN morphometry and concluded that subglacial erosion was likely a predominant formation mechanism. While there is strong evidence for historical mid-latitude glaciation and subglacial erosive processes provide a robust explanation for many of the VN characteristics that appear incompatible with surface/groundwater erosion [*Carr and Head III*, 2003; *Carr and Malin*, 2000; *Grau Galofre et al.*, 2020], the quantity, distribution, and dynamics of potential basal meltwater on Mars is largely unconstrained. *Fastook and Head* [2015] simulated the deposition and thermal evolution of ice sheets across the southern Noachian highlands and showed that basal temperatures can reach the melting point if the global water inventory of ancient Mars was at least five times larger than it is today. Ultimately *Fastook and Head* [2015] favor surface melt production brought about by 'heating events' which raise the atmospheric temperature above 273 K as the source of fluvial erosion, and thus do not investigate the volume of subglacial melt produced, its geographical association with VN, nor its dynamics.

The uncertainty in historical Martian climate, geothermal heat flux, and global water reservoir has led to conflicting conclusions about the feasibility of wet-based glaciation and hence subglacial hydrology (e.g., [*Butcher*, 2019; *Fastook and Head*, 2015; *Fastook et al.*, 2012; *Gallagher and Balme*, 2015]). However, mounting geomorphic (e.g., [*Butcher et al.*, 2017; *Carr and Head III*, 2003; *Carr and Malin*, 2000; *Gallagher and Balme*, 2015; *Grau Galofre et al.*, 2020; *Kargel and Strom*, 1992]) and mineralogical [*Ehlmann et al.*, 2011] evidence coupled with the difficulty in reconciling surface erosion and/or groundwater sapping in a cold, arid Noachian climate makes evaluating the consistency between putative basal melt patterns and VN distribution a potentially valuable investigation. Furthermore, improved estimates for Noachian geothermal heat fluxes [*Ojha et al.*, *2020*] have the potential to reveal novel insights into the likelihood and implications of subglacial processes on Mars. Namely, in addition to cyclic/transient fluvial processes, wet-based glaciation provides a rechargeable mechanism to explain the origin of VN in a cold, arid Martian climate. Additionally, the cyclic production of subglacial aqueous environments, analogous to Arctic or Antarctic subglacial systems, has numerous astrobiological implications [*Cockell et al.*, 2011; *Hays et al.*, 2017; *Mikucki et al.*, 2010; *Mikucki and Priscu*, 2004; *Mikucki et al.*, 2015; *Rutishauser et al.*, 2018].

To understand if wet-based glaciation could have carved Mars' VNs, we have expanded the capabilities of the one-dimensional, three-phase ice sheet evolution model of *Ojha et al.* [*2020*] to investigate the volume and distribution of basal melt produced during a variety of late Noachian icy highland scenarios. In Section 3.1 and 3.2 we constrain the geophysical and climatic conditions which permit basal melt volumes capable of carving the observed Martian VN and show that the global distribution of predicted basal melt is consistent with observations of VN distribution. In Sections 3.3 and 3.4 we implement a flow routing model to predict the morphometry of subglacial drainage channels and utilize fluvial metrics (Strahler stream order, stream elevation reversals) to determine their likely formation mechanisms. In Section 4 we discuss the geophysical, climatic, and astrobiological implication of our results, and highlight how targeted modeling investigations could provide additional insights into the evolution and habitability of relict, remnant, and modern ice-water environments on Mars.

2. Methods

2.1 Ice Sheet Model

To simulate the deposition, densification, and thermophysical evolution of Martian ice sheets we use the one-dimensional multiphase model of *Ojha et al.* [*2020*] (a summary of which can be found in Supplementary Section S1). The model simulates the evolving vertical temperature

and phase (ice, water, void space) profiles within an accreting ice sheet subject to thermal conduction, compaction, and basal melting processes. We have adapted the model to include latitudinally and altitudinally varying surface temperature, altitude dependent deposition of snow, and a supply limited total ice sheet volume (i.e., ice sheet volumes cannot exceed imposed global water inventories). Additionally, when basal melting occurs the melt is extracted from the model domain, returned to the global H_2O reservoir, and is available for redeposition onto the ice sheet. While lateral ice flow is not considered, basal melting and redeposition provide an ice sheet mass balance mechanism that can transport petatons of ice (Supplementary Figure S2) on timescales relevant to lateral ice transport across the coarse grid resolutions considered here (5 x 5 degrees ~ 300 km x 300 km, resulting in a timescale $t \sim l/u \sim l\mu r/\rho g h^3 \sim 30{,}000$ years, where l is our grid resolution [300 km], u is the radial spreading velocity of a gravitationally driven viscous thin film [9 m/yr], μ is viscosity [10^{13} Pa s], r is ice sheet radius [1000 km], ρ is ice density [900 kg/m^3], g is gravity [3.12 m/s^2], and h is ice sheet thickness [1 km]). As a number of environmental parameters affecting the model are not well constrained (e.g., historical global water reservoir, geothermal heat flux, regional glaciation patterns, water rock erosion ratios – i.e. the volume of water transported across a surface relative to the volume of rock eroded [*Carr and Malin*, 2000; *Lamb et al.*, 2006]), we simulate an array of potential scenarios and investigate the ensuing spatiotemporal evolution of ice sheet thickness and basal melt production.

The latitudinally and altitudinally dependent surface temperature implemented here is akin to that proposed by *Fastook and Head* [2015], and takes the form:

$$T_{surf}(lat, alt) = T_{surf}(lat) - c_1 alt \qquad (1)$$

where $T_{surf}(lat)$ is the latitude dependent surface temperature [K] proposed by *Wordsworth et al.* [2015] for an obliquity of 25° (digitized from Figure 1 of *Wordsworth et al.* [2015]), alt is the surface altitude [m] derived from 463 m resolution Mars Orbiter Laser Altimeter (MOLA) data, and c_1 is a constant coefficient (here 0.0012 K/m, chosen such that surface temperature distributions are consistent with *Wordsworth et al.* [2015]). A global surface temperature map can be seen in Figure 1a. Such a temperature distribution is consistent with contemporary estimates (e.g., [*Fastook and Head*, 2015; *Wordsworth et al.*, 2013]).

Altitude dependent snow deposition follows that of *Fastook and Head* [2015]:

$$b = \begin{cases} 0 & alt < 1000 \\ 0.01 * alt - 10 & if \quad 1000 \leq alt \leq 2000 \\ 10 & 2000 < alt \end{cases} \qquad (2)$$

Where b, deposition rate, is in mm/yr, and alt is in m. The upper snowfall limit of 10 mm/year is lower than arid terrestrial ice sheet systems (e.g., central Antarctica: ~50 mm/year water equivalent [*Bromwich et al.*, 2004]). Figure 1b shows the snow deposition map produced by Equation 2. We investigate the effects of regional ice sheet deposition in the mid latitudes (north of 60°S and south of 60°N). The intention is to simulate the glaciological cycling of ice away from the poles driven by obliquity, eccentricity and/or climate cycling (e.g., [*Madeleine et al.*, 2009; *Wordsworth et al.*, 2015]).

A conservative estimate of the present day global water reservoir of Mars is ~5 x 10^6 km^3 (~35 m thick global layer, accounting only for polar ice) [*Christensen*, 2006]. However, uncertainty in the rate of volatile outgassing in Mars' past, as well as the presence of deep cut

fluvial features, suggests that ancient Mars may have possessed a more substantial hydrosphere/cryosphere that has since been lost due to impact erosion and/or hydrodynamic escape [*Carr*, 1987; *Greenwood et al.*, 2008; *Jakosky et al.*, 2018]. As the current global water inventory does not lend itself to the formation of ice sheets thick enough to induce basal melting (e.g., [*Fastook and Head*, 2015; *Ojha et al.*, *2020*]), we explore global water inventories which range from 10-20 times that of the current Martian reservoir ($5 \cdot 10^7$-$1 \cdot 10^8$ km^3). This corresponds to a ~350-700 m thick global equivalent layer (GEL) of liquid water, at the lower end of Noachian water budget estimates (640-5000 m [*Luo et al.*, 2017; *Rosenberg et al.*, 2019]), providing a conservative estimate of the resultant subglacial water flux.

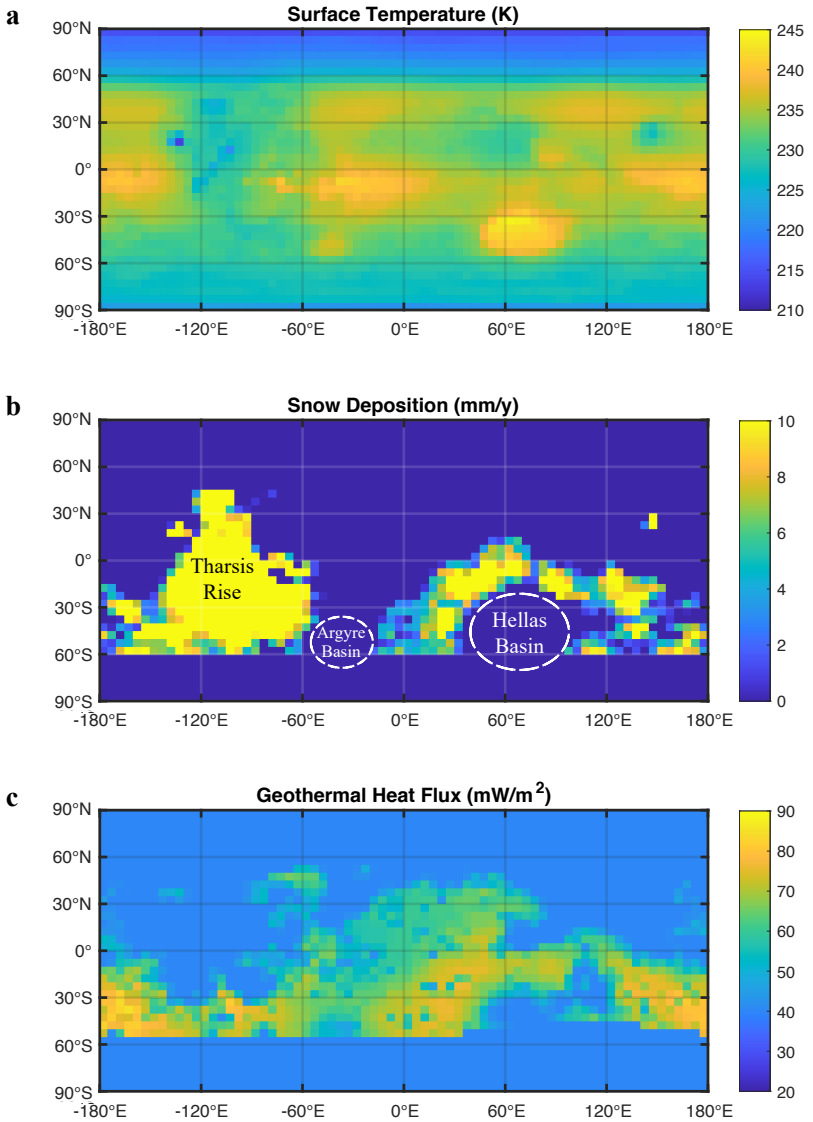

Figure 1 – Ice sheet model input parameters. **A)** Latitude and altitude dependent surface temperature distribution for a simulated Noachian Mars. **B)** Altitude dependent deposition of snow on a Noachian Mars, utilizing the deposition conditions of *Fastook and Head* [2015] (Equation 2) and restricting snow deposition to the mid-latitudes (north of 60°S and south of 60°N) to simulate obliquity driven glaciations. **C)** Global geothermal heat flux accounting for both crustal contributions and a 40 mW/m^2 mantle contribution. The crustal component of the heat flux is calculated using GRS data [*Ojha et al.*, *2020*].

An additional parameter that can substantially alter the amount of basal melt predicted by our model is the geothermal heat flux at the base of the ice sheet. Due to the lack of in situ estimates of Martian heat flow, any estimate of Noachian heat flow will have considerable uncertainties (see *Ojha et al.* [*2020*] for discussion). Thus, the goal here is to assess whether the currently constrained geophysical and geochemical properties of Mars, when extrapolated to the Noachian, could have allowed VN formation by subglacial melting. We adopt the geothermal heat flux maps predicted by *Ojha et al.* [*2020*] who utilize Mars Odyssey Gamma Ray Spectrometer measurements to estimate crustal heat flux and consider mantle heat flux contributions ranging from 20-40 mW/m^2 [*Ojha et al.*, 2019]. An example of a global geothermal heat flux map assuming a mantle heat flux contribution of 40 mW/m^2 is shown in Figure 1c. Polar geothermal heat flux estimates are not well constrained, resulting in a lack of accurate heat flux predictions in the region south of 60°S [*Ojha et al.*, *2020*] (the region excluded by our model).

Simulations are run on a 5 x 5 degree grid and are initiated without any ice present. Deposition of ice is governed by Equation 2 and we track the evolution of ice thickness and basal melt production during a hypothetical ten-million-year glaciological cycle (Section 3.1), providing ample time for the generation of fluvially carved valley features (e.g., [*Buhler et al.*, 2014]). Additional details on the model runs are included in the Supplement (Text S1).

2.2 Subglacial Hydrology

To investigate the dynamics of basal melt produced in our simulations we implement the digital elevation map (DEM) analysis software TopoToolbox [*Schwanghart and Kuhn*, 2010; *Schwanghart and Scherler*, 2014]. By combining the 463 m resolution MOLA data (downsampled to 1 km resolution) and the ice thicknesses calculated by our model, the hydraulic potential, ϕ [Pascal], beneath the ice sheet can be calculated [*Arnold et al.*, 2019; *Shreve*, 1972]:

$$\phi = \rho_w g z + k \rho_i g H \qquad (3)$$

where ρ_w is the density of the subglacial fluid (for pure water 1000 kg/m^3), g is gravity (3.711 m/s^2), z is bed elevation (from MOLA), k is a dimensionless flotation factor describing the influence of ice overburden pressure on the subglacial pressure (here $k = 1$, implying subglacial pressure is at the overburden pressure) [*Arnold et al.*, 2019], ρ_i is the density of ice (917 kg/m^3), and H is ice thickness. Gradients in this potential drive the flow of water beneath glaciers and ice sheets.

We use TopoToolbox to create a global flow map using the hydraulic potential (TopoToolbox employs the flow routing algorithm of *Tarboton* [1997]). Using the basal melt estimates from our model we produce global water accumulation maps, which represent the total volume of water that has flown over a grid cell (total upstream area multiplied by basal melt thickness) during the simulated ten-million-year glaciological cycle. Cells with lower hydraulic potentials will accumulate more flow and form channel structures like those seen on the Martian surface. From these accumulation maps we can investigate the predicted global distribution of subglacial channels and compare them with the distribution of observed valleys networks (Section 3.2). We use these simulated channel networks to calculate Strahler stream order and upstream gradient distributions, and we compare these geomorphic metrics to those of contemporary valley networks and terrestrial analogs (Sections 3.3-3.4). It is important to note that our use of contemporary Martian altimetry (even downsampled/smoothed data) will include signatures of present-day VN topography (i.e., $\rho_w g z$ of Equation 3). As such, we emphasize the model's

predictions of global and regional VN distribution over localized channelization patterns. However, agreement between predicted and observed VN distribution at the local scale ensures the applicability of the morphometric analysis, as calculations of stream order and along-channel gradient of simulated VN should be coincident with existing VN.

3. Results

3.1 Ice Thickness and Basal Melt

To test the sensitivity of ice sheet thickness and basal melt production to variations in mantle heat flux and global water reservoir volume, we simulated the deposition and evolution of Martian ice sheets using 9 unique sets of input parameters (mantle heat fluxes of 20-40 mW m^{-2} and global water reservoirs of $5 \cdot 10^7$-$1 \cdot 10^8$ km^3; Figure 2a). As an example, Figure 2b-c shows global maps of ice thickness and total basal melt at the end of a 10-million-year simulation with 40 mW/m^2 mantle heat flux and 20x the present-day global water reservoir. Ice sheets with thicknesses up to ~4 km are produced during the simulations.

The likelihood that basal melting will occur under a given scenario is shown in the regime diagram of Figure 2a. In all but one scenario the ice sheets either do not produce any basal melt (Regime I) or approach a cold based equilibrium after a period of transient basal melting (Regime II). This result is likely accentuated by the lack of lateral ice flow and sublimation in our ice sheet model, preventing the motion of ice to lower altitudes where it would sublimate, be reintroduced into the global water reservoir, and again be deposited in regions that can sustain basal melting. Instead, the ice sheet continues to thicken over regions which do not sustain basal melting, draining the global water reservoir and stagnating basal melt production. For these reasons, our results provide a lower bound for basal melt production. The one simulation which does not result in a cold base equilibrium (40 mW/m^2, 20x reservoir), reaches a different steady state in which basal melt production becomes constant (Regime III). In this case the ice sheet reaches a global steady state thickness that supports ongoing regional basal melting (Supplementary Figure S2). Total basal melt production estimates across these nine simulations range from $6.22 \cdot 10^4$ km^3 to $2.11 \cdot 10^8$ km^3.

The estimated volume of water necessary to carve all of the observed VN on Mars, using a 1000:1 water to rock erosion ratio (based on the slow erosion of basalt [*Gulick and Baker*, 1993]), is ~9 x 10^7 km^3 (using the 146,000 km estimated total length of Noachian VN and valley volume estimation method of *Carr and Malin* [2000]). In many of the larger reservoir runs the total basal melt produced is on the same order as, or exceeds, this volume estimate (Figure 2a). This suggest that if ancient Mars possessed a water reservoir 15 to 20 times greater than the conservative modern-day estimate, the VN of Mars could have been incised by basal melt produced during cyclic glaciations, even under cold and dry climate conditions.

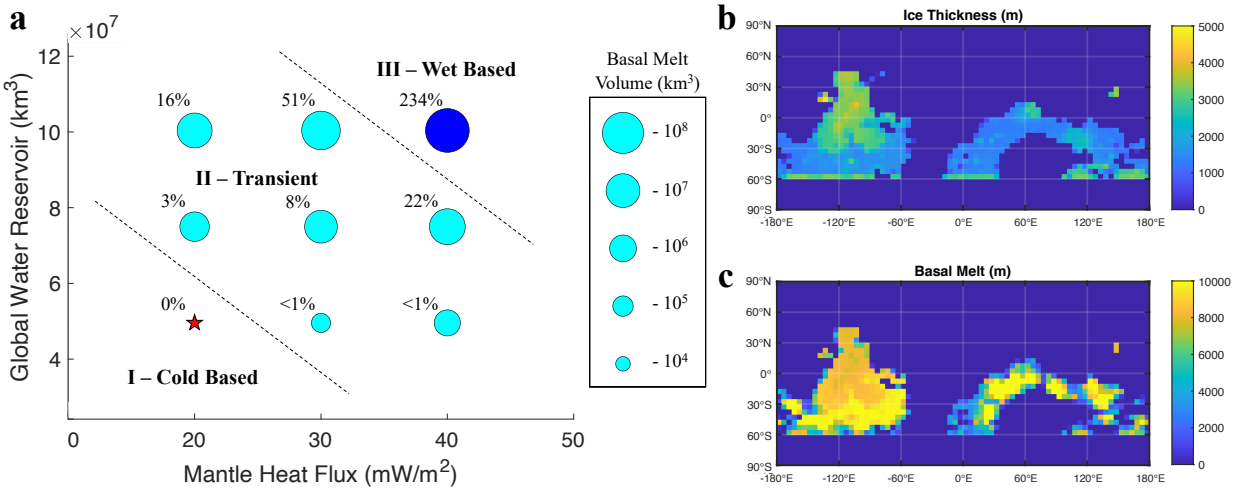

Figure 2 – Ice sheet and basal melt characteristics. **a)** Regime diagram for the nine simulated ice sheet scenarios. Regime I: Cold based glaciation where no basal melting occurs. Regime II: Transient basal melting occurs before a cold based steady state is reached. Regime III: Wet based glaciation where the ice sheet in its steady state continues to produce basal melt. Percentages represent the fraction of total water needed to erode the observed valley networks (based on the 9 x 10^7 km^3 estimate of *Carr and Malin* [2000]). (Note: dashed lines indicate approximate divisions in melt regimes.) **b-c)** Global distribution of ice thickness (b) and total basal melt production (c) at the end of a simulated 10 Ma glacial cycle with a 40 mW/m^2 mantle heat flux and 20x global water reservoir.

3.2 Channel Distribution

To compare the distribution of simulated subglacial drainage channels to identified VN on Mars we coplot the known locations of VN [*Hynek et al.*, 2010] with the hydraulic head driven subglacial flow map (Figure 3a). We use basal melt and ice thickness quantities from the simulation with a 40 mW/m^2 mantle heat flux and a 20x global water reservoir (the sole wet based glaciation scenario – Figure 2a). Channels in the subglacial flow map are identified by setting an accumulation tolerance, such that an appreciable amount of basal melt must flow through a domain element before it is deemed a channel. Here, we set this tolerance to the amount of water required for a channel to incise through 1 km of rock, assuming a water rock erosion ratio of 1000:1. For comparison we also include high resolution maps of selected regions where an accumulation tolerance of 100 m is utilized (Figure 3b-c and Supplementary Figure S3). Implementing a lower accumulation tolerance results in finer scale upstream channel structures being included (more small-scale tributaries). There is good agreement between our simulated channel distribution and the observed distribution of VN, with a few notable exceptions. In general, the majority of channels are restricted to the Noachian highlands, with high valley densities north and northeast of Hellas Basin and south of Tharsis Rise, while there exists a dearth of valleys near Argyre Basin. Our model overpredicts channel distributions on Tharsis Rise as well as to the immediate west of Hellas Basin, while underpredicting the number of channels in Arabia Terra. Possible causes for such discrepancies as well as implications of the more prevalent agreement in regional distribution are discussed in Section 4.

3.3 Stream Order

Strahler stream order is a measure of the complexity of branching channel networks [*Strahler*, 1957]. In brief, headwater tributaries are categorized as first-order streams and upon confluence with another first-order stream become second-order streams. Second-order streams remain second-order until they meet another second-order stream, at which point the channel

downstream of the confluence is defined as third-order. These are examples of the principal rule in this ordering scheme: stream order increases by one wherever channels of the same order merge (Supplementary Figure S4).

In terrestrial river networks, the number of streams of order ω, N_ω, tends to decrease geometrically with stream order (N_ω / $N_{\omega-1}$ = R_B, where R_B is a constant termed the bifurcation ratio; [*Horton*, 1945]). This property is shared by nearly all channel networks, including those that are topologically random [*Kirchner*, 1993]. Recent studies have postulated that channels carved by distinct erosive processes (e.g., fluvial, glacial, subglacial, ground sapping) should exhibit different Strahler stream order distributions [*Grau Galofre and Jellinek*, 2017; *Grau Galofre et al.*, 2020; *Grau Galofre et al.*, 2018; *Storrar et al.*, 2014]. If true, these should manifest as differences in R_B and the cumulative distribution function of the number of streams by stream order.

Here, we examine the Strahler stream orders of our simulated subglacial drainage network as well as those of mapped VN [*Hynek et al.*, 2010] and compare these to the Strahler stream order distribution of terrestrial river and esker systems [*Downing et al.*, 2012; *Storrar et al.*, 2014] (Figure 3d). We computed these with several erosion tolerances – the requirement that enough water flow over a grid cell to erode it to a certain depth before it is considered a channel – ranging from 1 to 1000 m. In the cumulative distribution function plot in Figure 3d, erosion values correspond to the erosion tolerance utilized to determine what constitutes a channel (using the 1000:1 water to rock erosion ratio discussed above). Bifurcation ratios averaged across all stream orders are R_{Earth}=0.21, R_{Eskers}=0.24, R_{Mars}=0.30, R_{1m}=0.51, R_{10m}=0.53, R_{100m}=0.54, and R_{1000m}=0.55 for terrestrial rivers and eskers, observed Martian VN, and simulated channels using erosions tolerances of 1-1000 m, respectively.

Both modeled and observed Martian channel networks have fewer tributaries than terrestrial river systems [*Downing et al.*, 2012; *Leopold et al.*, 2020]. This could be attributed to the erasure of small channels (<100 m width) over time [*Hynek et al.*, 2010] or may indicate a formation mechanism that produces a lower proportion of tributary structures, such as subglacial drainage channels (evidenced by the lower number of first-order channels observed for terrestrial eskers – Figure 3d). The coincidence of observed first-order channels (red dashed line of Figure 3d) and first-order channels produced using a 100 m accumulation tolerance could indicate that ~ 100 m of hillslope erosion has occurred since the incision of the VN (erasing shallower first-order channels predicted using 1 m and 10 m accumulation tolerances) and explain why small valley structures are missing from the geologic record. Comparison of the expected to observed crater populations of the same scale (~100 m) could provide a method for testing this hypothesis, as a similar dearth of small craters would be expected. The larger bifurcation ratios of both observed and simulated VN, compared to R_{Earth}, could indicate a formation mechanism that differs from the primarily subaerial processes carving rivers and streams on Earth. That said, Strahler stream order alone does not provide substantial evidence to identify a specific formation mechanism [*Kirchner*, 1993].

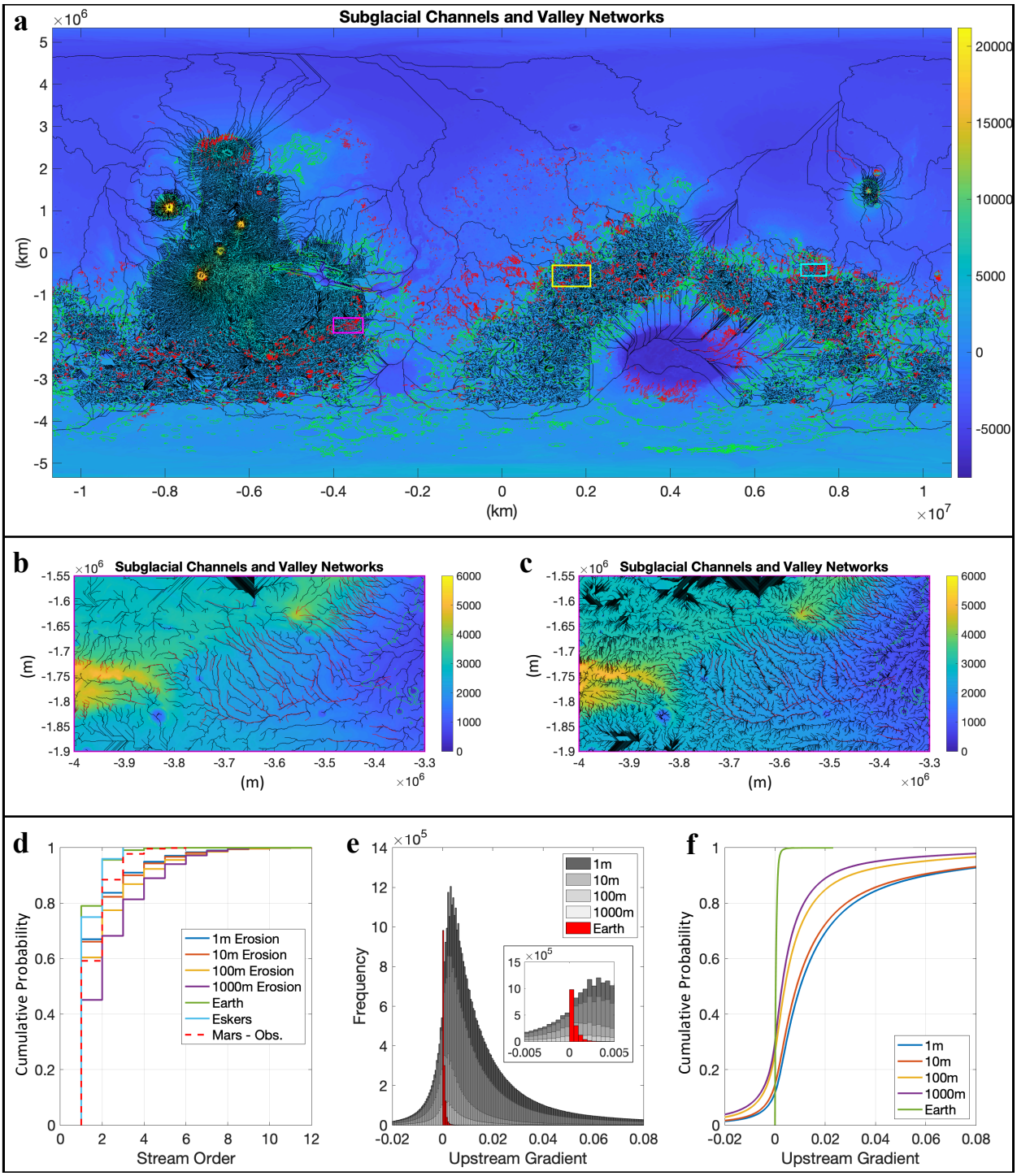

Figure 3 – Distribution and geomorphometric characteristics of simulated and observed VN. **a)** Comparison of the global distribution of simulated subglacial channels and observed VN [*Hynek et al.*, 2010]. Locations of channels simulated by our model (black) and identified VN from *Hynek et al.* [2010] (red) are generally consistent, with high densities in the mid-latitude Noachian highlands. An erosion tolerance of 1000 m was implemented. The green contour line indicates an elevation of 1000 m, below which no ice sheet accumulation will occur (Equation 2). Fine-scale channel structure and further agreement between observations and model results can be seen in high resolution images of regions bounded by the magenta (3b-c), cyan, and yellow rectangles (Supplementary Figure S3). Colorbars indicate elevation (m) from MOLA data. **b-c)** Comparison of modeled channels (black) and observed VN (red) for the region south of Valles Marineris outlined by the magenta rectangle, computed using erosion tolerances of 1000 m (b) and

100 m (c). **d)** Cumulative distribution functions of Strahler stream orders in Martian and terrestrial hydrologic systems. Entries labeled '1-1000 m Erosion' correspond to modeled channel networks with erosion tolerances of 1-1000 m. 'Earth' represents global Strahler stream orders for terrestrial river systems [*Downing et al.*, 2012]. 'Eskers' represents Strahler stream orders for eskers in northern Canada [*Storrar et al.*, 2014]. 'Mars – Obs' represents Strahler stream orders for observed Martian VN [*Hynek et al.*, 2010]. **e)** Upstream basal gradient of simulated subglacial channels and terrestrial river systems. Values less than zero correspond to regions along simulated channels where hydraulic potential drives uphill flow. (Inset – magnified view near zero gradient) **f)** Upstream gradient cumulative distribution functions for the data in Figure 3e. A lower probability at an upstream gradient of zero for 1 m and 10 m simulations suggests that tributary flow is more likely to follow bedrock topography than is main channel flow.

3.4 Channel Gradient

A more robust indicator of subglacial channel flow is the tendency for portions of the drainage network to flow uphill. Subglacial hydrology is driven by hydraulic potential, which is affected by both bed topography and overlying ice thickness (see Equation 3). Because of this, basal melt flows along potential gradients, even if these are against the topographic gradients of the bed. This is a dynamic unique to subglacial flow as subaerial flow always follows topography [*Grau Galofre and Jellinek*, 2017; *Grau Galofre et al.*, 2020; *Grau Galofre et al.*, 2018; *Storrar et al.*, 2014].

Here we calculate the upstream gradients for our simulated channel systems using erosion tolerances of 1 m, 10 m, 100 m, and 1000 m. We show a histogram and cumulative distribution function plot of upstream gradients for all erosion scenarios as well as observed terrestrial values for all rivers wider than 90 m [*Frasson et al.*, 2019] in Figure 3e-f. The occurrence of negative upstream gradients in our simulated channel systems range from ~12-30% of the total channel length depending on the erosion tolerance employed. The consistent overlap of our simulated channels and those identified from orbital images (e.g., Figure 3b-c) suggests that a proportional amount of observed valley networks likely exhibit uphill drainage patterns. Indeed, this is consistent with the measurements of multiple longitudinal profile reversals made by *Grau Galofre et al.* [2020] across 10,276 Martian valley segments. Conversely, as expected, terrestrial rivers do not exhibit negative upstream gradients. While the bias of larger rivers in the database of *Frasson et al.* [2019] skews the distribution towards shallower gradients (a similar trend can be observed for our simulated subglacial channels in Figure 3e as the erosion tolerance is increased), the dearth of negative upstream slopes in subaerial terrestrial systems is self-evident. The significant presence of negative upstream gradients, incompatible with a subaerial origin, is consistent with the argument that subglacial processes could have played a substantial role in incising Mars' VN.

4. Discussion

By simulating the deposition and thermophysical evolution of Late Noachian icy highlands (LNIH) ice sheets with updated geothermal heat flux estimations we have shown that with a substantial global water reservoir, basal melting of Mars' glaciers is possible and can explain the observed VN. The regional distribution and volume of the basal melt produced is consistent with the distribution of observed VN on the Martian surface and the estimated volume of water necessary to erode these valleys. This is true for both large global water reservoirs with high geothermal heat flux as well as smaller reservoirs with lower geothermal heat flux as cyclic glaciations forced by obliquity and eccentricity variations could produce repetitive erosive periods, deepening channels over time [*Byrne*, 2009; *Madeleine et al.*, 2009; *Wordsworth et al.*, 2013]. Additionally, our total basal melt estimates are lower bounds, and the actual volumes are likely to be higher for all scenarios. Typical modeled ice sheet thicknesses (with the exception of those in

the Tharsis Rise region – discussed below) are ~1-3 km, which is within the range predicted by contemporary estimates of LNIH scenarios [*Cassanelli and Head*, 2015; *Fastook and Head*, 2015].

While our results require a larger global water reservoir than is currently available on Mars (345-690 m GEL), the historical water inventory of Mars is largely unconstrained and estimates for the available near-surface water reservoir during the Noachian range from a 24-5000 m global equivalent layer (GEL) [*Carr and Head*, 2015; *Kurokawa et al.*, 2014; *Luo et al.*, 2017]. Given this uncertainty in Mars' historical climate and the number of VN morphological properties consistent with subglacial processes, we find it instructive to reinvestigate the feasibility and dynamics of basal melt production in greater detail. A subglacial origin for Mars' VN is particularly advantageous given the possibility that ancient Mars was cold and arid, precluding the heightened surface temperatures needed to reconcile surface melting/precipitation driven erosion as the sole formation mechanism for VN incision (e.g., [*Fastook and Head*, 2015]). On the other hand, geothermal heat flow during the Noachian eon would have undoubtedly been much higher than at the present, delivering thermal energy to the base of any existing ice sheets. Moreover, morphometric characteristics of our simulated channel systems (upstream gradient and to a lesser extent Strahler stream order and bifurcation ratio) are consistent with features of terrestrial subglacial drainage systems and VN observations [*Grau Galofre and Jellinek*, 2017; *Grau Galofre et al.*, 2020; *Grau Galofre et al.*, 2018; *Hynek et al.*, 2010; *Storrar et al.*, 2014]. Groundwater sapping may also play a role in VN formation (e.g., [*Gulick*, 2001]), although definitive evidence for the ability of spring flow to excavate the volumes observed on Mars as well as the often invoked unique relation between amphitheater headwall morphometries and groundwater seepage has been shown to be lacking in bedrock canyons [*Lamb et al.*, 2006; *Lapotre and Lamb*, 2018]. *Lapotre et al.* [2016] instead suggest that catastrophic outburst floods may be responsible for Mars' steep headwalled canyons. Basal melting beneath ice sheets and subglacial floods (or Jökulhlaups) could potentially source such catastrophic fluvial events on Mars [*Evatt et al.*, 2006], even in a Noachian climate with low precipitation rates.

There are limitations to our current one-dimensional ice sheet model, which likely contribute to a number of inconsistencies between observed VN distribution and our simulated channel networks. First, the lack of lateral ice transport between model grid cells (discussed in Section 3.1) reduces the total amount of basal melt produced by preventing downslope transport of ice via viscous flow and resultant sublimation, which could recharge ice sheets and amplify total basal melt estimates. Moreover, multidimensional basal hydrology models (e.g., [*Sommers et al.*, 2018]) would provide insight into the multiscale temporal evolution of the subglacial channel environment.

Second, we employ a simplified deposition scenario which does not allow for snow deposition below 1000 m in altitude. This limits the opportunities for valley incision in lower lying areas (e.g., Arabia Terra, Hellas Basin) to larger outflow channels flowing down from regions with ice cover, resulting in the underprediction of VN densities in these areas and a handful of unlikely channels in the northern lowlands (an artifact of the flow routing algorithm, which extends flow paths to the edge of the DEM). Similarly, our deposition model does not account for any atmosphere or climate dynamic impacts on longitudinally varying snow accumulation, nor does it consider the possibility of true polar wander induced reorientation [*Bouley et al.*, 2016]. It has been demonstrated that climate forcing could lead to heterogenous deposition of snow/ice with amplifications in specific regions (e.g. [*Madeleine et al.*, 2009; *Wordsworth et al.*, 2015]). Alternatively, *Bouley et al.* [2016] show that a reorientation of Mars' spin axis due to the formation of the Tharsis region leads to the clustering of Noachian era VN around a common historic latitude

of 24°S which excludes the present day region west of Hellas Basin. Thus, our overprediction of channel density west of Hellas Basin could be the result of regionally overestimated snow deposition, facilitating the unrealistic accumulation of an ice sheet thick enough to induce basal melting.

Another region that is not well captured by the model is Tharsis Rise. Due to its high elevations, Tharsis Rise accretes substantial snow and produces enough basal melt to incise channels over much of its surface. In reality, Tharsis Rise is mostly void of channel structures, except for locally around Mons peaks. The region has been geologically reworked since the Noachian era, both by uplift and resurfacing processes [*Bouley et al.*, 2016], which our model does not capture. As a result, we drastically overpredict the presence of channels in this region.

Lastly, we do not account for historical topographical changes due to postglacial rebound of the Martian lithosphere after the melting of the LNIH ice sheet, global deformation caused by true polar wander [*Creveling et al.*, 2012; *Perron et al.*, 2007], dynamic topography [*Roberts and Zhong*, 2004], or topographic responses to changes in sediment loading. These processes could significantly impact the results of the predicted flow paths, most notably the observed negative upstream channel gradients, as Mars' contemporary topography could have been substantially reworked since its exhumation from beneath a thick LNIH ice sheet. Thus, while our simulated channel gradient distributions (Figure 3e-f) are consistent with subglacial channel formation, the presence of negative upstream gradients may also be consistent with large-scale topographic deformation from a number of other processes (e.g., glacial isostatic adjustment, true polar wander, dynamic topography, etc.). Future work incorporating these processes could be compared with our current distribution of negative upstream channel gradients to identify if particular deformation mechanisms could account for the observed trends in channel profile reversals.

While the current model is idealized, it provides a novel and versatile tool to investigate the thermophysical evolution of depositional planetary ices. The three-phase nature of the model, which accurately accounts for the latent heat associated with basal melting, constitutes a robust, yet simple, method of simulating Martian ice deposits that extends the capabilities of current models. The model is adaptable and can easily be modified to investigate both high resolution regional and coarse resolution global ice sheet processes throughout Mars' history. Additionally, the model is primed to accommodate improvements (e.g. climate model driven deposition [*Madeleine et al.*, 2009], seasonal/obliquity/eccentricity driven surface temperature variations [*Wordsworth et al.*, 2013; *Wordsworth*, 2016; *Wordsworth et al.*, 2015], additional phases [sediment] to simulate ground ice evolution [*Bramson et al.*, 2015], lateral ice flow, and simulation of saline/hypersaline subglacial fluids [*Lauro et al.*, 2020; *Sori and Bramson*, 2019]).

The model highlights the potential for geothermally driven basal melt production beneath thick ice deposits and demonstrates that morphometric properties of the resultant subglacial drainage channels are consistent with observed VN characteristics indicative of glacially related erosion [*Grau Galofre and Jellinek*, 2017; *Grau Galofre et al.*, 2020]. These consistencies, along with the uncertainty in Mars' historic global water reservoir and potentially cold arid past, makes reassessing a subglacial origin for Mars' VN of appreciable interest as this could resolve many issues associated with fluvial feature generation given the faint young sun paradox [*Haberle*, 1998; *Ojha et al.*, *2020*]. The identification of subglacially modified pre-LNIH impact features (e.g. [*Yin et al.*, 2021]) would strengthen the evidence for a dynamic, potentially wet-based, LNIH scenario. Furthermore, identifying regions that can sustain aqueous environments, both historically and currently (e.g., beneath the south polar layered deposits [*Lauro et al.*, 2020; *Orosei et al.*, 2018]),

constraining their longevity, and understanding their dynamics has substantial astrobiological implications for both planetary exploration and planetary protection.

5. Conclusion

By combining improved estimates of geothermal heat flux and a novel model of ice sheet thermophysical evolution, we demonstrate that the basal melting of a Noachian era ice sheet could facilitate subglacial processes capable of forming Mars' valley networks. Morphological characteristics of our simulated channel systems (upstream gradient and Strahler stream order) corroborate observational evidence extracted from orbital observations of valley networks [*Grau Galofre et al.*, 2020; *Hynek et al.*, 2010] which suggests they may have a subglacial erosion driven origin. The consistency with observed glaciofluvial features, agreement with global valley network distribution, and ability to reconcile channel formation on a cold, arid early Mars suggests subglacial processes could play a larger role in the geophysical evolution and spatiotemporal habitability of Mars than previously thought.

6. References

Arnold, N. S., S. J. Conway, F. E. Butcher, and M. R. Balme (2019), Modeled subglacial water flow routing supports localized intrusive heating as a possible cause of basal melting of Mars' south polar ice cap, *Journal of Geophysical Research: Planets*, *124*(8), 2101-2116.

Bouley, S., D. Baratoux, I. Matsuyama, F. Forget, A. Séjourné, M. Turbet, and F. Costard (2016), Late Tharsis formation and implications for early Mars, *Nature*, *531*(7594), 344-347.

Bramson, A. M., S. Byrne, N. E. Putzig, S. Sutton, J. J. Plaut, T. C. Brothers, and J. W. Holt (2015), Widespread excess ice in Arcadia Planitia, Mars, *Geophysical Research Letters*, *42*(16), 6566-6574.

Bromwich, D. H., Z. Guo, L. Bai, and Q.-s. Chen (2004), Modeled Antarctic precipitation. Part I: Spatial and temporal variability, *Journal of Climate*, *17*(3), 427-447.

Buhler, P. B., C. I. Fassett, J. W. Head III, and M. P. Lamb (2014), Timescales of fluvial activity and intermittency in Milna Crater, Mars, *Icarus*, *241*, 130-147.

Butcher, F. E. (2019), Wet-Based Glaciation on Mars, The Open University.

Butcher, F. E., M. R. Balme, C. Gallagher, N. S. Arnold, S. J. Conway, A. Hagermann, and S. R. Lewis (2017), Recent basal melting of a mid-latitude glacier on Mars, *Journal of Geophysical Research: Planets*, *122*(12), 2445-2468.

Byrne, S. (2009), The polar deposits of Mars, *Annual Review of Earth and Planetary Sciences*, *37*.

Carr, M., and J. Head (2015), Martian surface/near-surface water inventory: Sources, sinks, and changes with time, *Geophysical Research Letters*, *42*(3), 726-732.

Carr, M. H. (1987), Water on Mars, *Nature*, *326*(6108), 30-35, doi:DOI 10.1038/326030a0.

Carr, M. H., and J. W. Head III (2003), Basal melting of snow on early Mars: A possible origin of some valley networks, *Geophysical Research Letters*, *30*(24).

Carr, M. H., and M. C. Malin (2000), Meter-scale characteristics of Martian channels and valleys, *Icarus*, *146*(2), 366-386.

Cassanelli, J. P., and J. W. Head (2015), Firn densification in a Late Noachian "icy highlands" Mars: Implications for ice sheet evolution and thermal response, *Icarus*, *253*, 243-255.

Christensen, P. R. (2006), Water at the poles and in permafrost regions of Mars, *Elements*, *2*(3), 151-155.

554 Cockell, C. S., E. Bagshaw, M. Balme, P. Doran, C. P. McKay, K. Miljkovic, D. Pearce, M. J.
555 Siegert, M. Tranter, and M. Voytek (2011), Subglacial environments and the search for
556 life beyond the Earth, *Antarctic Subglacial Aquatic Environments*, *192*, 129-148.
557 Creveling, J., J. Mitrovica, N.-H. Chan, K. Latychev, and I. Matsuyama (2012), Mechanisms for
558 oscillatory true polar wander, *Nature*, *491*(7423), 244-248.
559 Downing, J. A., J. J. Cole, C. Duarte, J. J. Middelburg, J. M. Melack, Y. T. Prairie, P.
560 Kortelainen, R. G. Striegl, W. H. McDowell, and L. J. Tranvik (2012), Global abundance
561 and size distribution of streams and rivers, *Inland waters*, *2*(4), 229-236.
562 Ehlmann, B. L., J. F. Mustard, S. L. Murchie, J.-P. Bibring, A. Meunier, A. A. Fraeman, and Y.
563 Langevin (2011), Subsurface water and clay mineral formation during the early history of
564 Mars, *Nature*, *479*(7371), 53-60.
565 Evatt, G., A. Fowler, C. Clark, and N. Hulton (2006), Subglacial floods beneath ice sheets,
566 *Philosophical Transactions of the Royal Society A: Mathematical, Physical and*
567 *Engineering Sciences*, *364*(1844), 1769-1794.
568 Fastook, J. L., and J. W. Head (2015), Glaciation in the Late Noachian Icy Highlands: Ice
569 accumulation, distribution, flow rates, basal melting, and top-down melting rates and
570 patterns, *Planetary and Space Science*, *106*, 82-98, doi:10.1016/j.pss.2014.11.028.
571 Fastook, J. L., J. W. Head, D. R. Marchant, F. Forget, and J.-B. Madeleine (2012), Early Mars
572 climate near the Noachian–Hesperian boundary: Independent evidence for cold
573 conditions from basal melting of the south polar ice sheet (Dorsa Argentea Formation)
574 and implications for valley network formation, *Icarus*, *219*(1), 25-40.
575 Frasson, R. P. d. M., T. M. Pavelsky, M. A. Fonstad, M. T. Durand, G. H. Allen, G. Schumann,
576 C. Lion, R. E. Beighley, and X. Yang (2019), Global database of river width, slope,
577 catchment area, meander wavelength, sinuosity, and discharge.
578 Gallagher, C., and M. Balme (2015), Eskers in a complete, wet-based glacial system in the
579 Phlegra Montes region, Mars, *Earth and Planetary Science Letters*, *431*, 96-109.
580 Grau Galofre, A., and A. M. Jellinek (2017), The geometry and complexity of spatial patterns of
581 terrestrial channel networks: Distinctive fingerprints of erosional regimes, *Journal of*
582 *Geophysical Research: Earth Surface*, *122*(4), 1037-1059.
583 Grau Galofre, A., A. M. Jellinek, and G. R. Osinski (2020), Valley formation on early Mars by
584 subglacial and fluvial erosion, *Nature Geoscience*, 1-6.
585 Grau Galofre, A., M. Jellinek, G. Osinski, M. Zanetti, and A. Kukko (2018), Subglacial drainage
586 patterns of Devon Island, Canada: detailed comparison of rivers and subglacial meltwater
587 channels.
588 Greenwood, J. P., S. Itoh, N. Sakamoto, E. P. Vicenzi, and H. Yurimoto (2008), Hydrogen
589 isotope evidence for loss of water from Mars through time, *Geophysical Research*
590 *Letters*, *35*(5).
591 Gulick, V., and V. Baker (1993), Fluvial valleys in the heavily cratered terrains of Mars:
592 Evidence for paleoclimatic change?, paper presented at Early Mars: How Warm and How
593 Wet?
594 Gulick, V. C. (2001), Origin of the valley networks on Mars: A hydrological perspective,
595 *Geomorphology*, *37*(3-4), 241-268.
596 Haberle, R. M. (1998), Early Mars climate models, *Journal of Geophysical Research-Planets*,
597 *103*(E12), 28467-28479, doi:Doi 10.1029/98je01396.

598 Haberle, R. M., K. Zahnle, N. G. Barlow, and K. E. Steakley (2019), Impact degassing of H2 on
599 early Mars and its effect on the climate system, *Geophysical Research Letters*, *46*(22),
600 13355-13362.
601 Hays, L. E., H. V. Graham, D. J. Des Marais, E. M. Hausrath, B. Horgan, T. M. McCollom, M.
602 N. Parenteau, S. L. Potter-McIntyre, A. J. Williams, and K. L. Lynch (2017),
603 Biosignature preservation and detection in Mars analog environments, *Astrobiology*,
604 *17*(4), 363-400.
605 Head, J. W., and D. R. Marchant (2014), The climate history of early Mars: insights from the
606 Antarctic McMurdo Dry Valleys hydrologic system, *Antarctic Science*, *26*(6), 774-800.
607 Hewitt, I. J. (2011), Modelling distributed and channelized subglacial drainage: the spacing of
608 channels, *Journal of Glaciology*, *57*(202), 302-314.
609 Horton, R. E. (1945), Erosional development of streams and their drainage basins; hydrophysical
610 approach to quantitative morphology, *Geological society of America bulletin*, *56*(3), 275-
611 370.
612 Hynek, B. M., M. Beach, and M. R. Hoke (2010), Updated global map of Martian valley
613 networks and implications for climate and hydrologic processes, *Journal of Geophysical*
614 *Research: Planets*, *115*(E9).
615 Jakosky, B., D. Brain, M. Chaffin, S. Curry, J. Deighan, J. Grebowsky, J. Halekas, F. Leblanc, R.
616 Lillis, and J. Luhmann (2018), Loss of the Martian atmosphere to space: Present-day loss
617 rates determined from MAVEN observations and integrated loss through time, *Icarus*,
618 *315*, 146-157.
619 Kargel, J. S., V. R. Baker, J. E. Begét, J. F. Lockwood, T. L. Péwé, J. S. Shaw, and R. G. Strom
620 (1995), Evidence of ancient continental glaciation in the Martian northern plains, *Journal*
621 *of Geophysical Research: Planets*, *100*(E3), 5351-5368.
622 Kargel, J. S., and R. G. Strom (1992), Ancient glaciation on Mars, *Geology*, *20*(1), 3-7.
623 Kirchner, J. W. (1993), Statistical inevitability of Horton's laws and the apparent randomness of
624 stream channel networks, *Geology*, *21*(7), 591-594.
625 Kurokawa, H., M. Sato, M. Ushioda, T. Matsuyama, R. Moriwaki, J. M. Dohm, and T. Usui
626 (2014), Evolution of water reservoirs on Mars: Constraints from hydrogen isotopes in
627 martian meteorites, *Earth and Planetary Science Letters*, *394*, 179-185.
628 Lamb, M. P., A. D. Howard, J. Johnson, K. X. Whipple, W. E. Dietrich, and J. T. Perron (2006),
629 Can springs cut canyons into rock?, *Journal of Geophysical Research: Planets*, *111*(E7).
630 Lapotre, M. G., and M. P. Lamb (2018), Substrate controls on valley formation by groundwater
631 on Earth and Mars, *Geology*, *46*(6), 531-534.
632 Lapotre, M. G., M. P. Lamb, and R. M. Williams (2016), Canyon formation constraints on the
633 discharge of catastrophic outburst floods of Earth and Mars, *Journal of Geophysical*
634 *Research: Planets*, *121*(7), 1232-1263.
635 Lauro, S. E., et al. (2020), Multiple subglacial water bodies below the south pole of Mars
636 unveiled by new MARSIS data, *Nature Astronomy*, doi:10.1038/s41550-020-1200-6.
637 Leopold, L. B., M. G. Wolman, J. P. Miller, and E. Wohl (2020), *Fluvial processes in*
638 *geomorphology*, Dover Publications.
639 Lucchitta, B. K., D. M. Anderson, and H. Shoji (1981), Did ice streams carve martian outflow
640 channels?, *Nature*, *290*(5809), 759-763.
641 Luo, W., X. Cang, and A. D. Howard (2017), New Martian valley network volume estimate
642 consistent with ancient ocean and warm and wet climate, *Nature communications*, *8*(1),
643 1-7.

644 Luo, W., and T. Stepinski (2009), Computer-generated global map of valley networks on Mars,
645 *Journal of Geophysical Research: Planets*, *114*(E11).
646 Madeleine, J.-B., F. Forget, J. W. Head, B. Levrard, F. Montmessin, and E. Millour (2009),
647 Amazonian northern mid-latitude glaciation on Mars: A proposed climate scenario,
648 *Icarus*, *203*(2), 390-405.
649 Meyer, C. R., M. C. Fernandes, T. T. Creyts, and J. R. Rice (2016), Effects of ice deformation on
650 Röthlisberger channels and implications for transitions in subglacial hydrology, *Journal*
651 *of Glaciology*, *62*(234), 750-762.
652 Mikucki, J., W. B. Lyons, I. Hawes, B. D. Lanoil, and P. T. Doran (2010), Saline lakes and
653 ponds in the McMurdo Dry Valleys: ecological analogs to Martian paleolake
654 environments, *Life in Antarctic Deserts and Other Cold Dry Environments:*
655 *Astrobiological Analogs*, 160-194.
656 Mikucki, J., and J. Priscu (2004), Microbial life in Blood Falls: an ancient Antarctic ecosystem,
657 paper presented at Proc. 2nd Conf. on Early Mars.
658 Mikucki, J. A., E. Auken, S. Tulaczyk, R. Virginia, C. Schamper, K. Sørensen, P. Doran, H.
659 Dugan, and N. Foley (2015), Deep groundwater and potential subsurface habitats beneath
660 an Antarctic dry valley, *Nature communications*, *6*(1), 1-9.
661 Milton, D. J. (1973), Water and processes of degradation in the Martian landscape, *Journal of*
662 *Geophysical Research*, *78*(20), 4037-4047.
663 Ojha, L., J. Buffo, S. Karunatillake, and M. Siegler (*2020*), Groundwater Production from
664 Geothermal Heating on Early Mars and Implications for Early Matian Habitability,
665 *Science advances*.
666 Ojha, L., S. Karimi, K. W. Lewis, S. E. Smrekar, and M. Siegler (2019), Depletion of Heat
667 Producing Elements in the Martian Mantle, *Geophysical Research Letters*, *46*(22),
668 12756-12763.
669 Orosei, R., et al. (2018), Radar evidence of subglacial liquid water on Mars, *Science*, *361*(6401),
670 490-493, doi:10.1126/science.aar7268.
671 Perron, J. T., J. X. Mitrovica, M. Manga, I. Matsuyama, and M. A. Richards (2007), Evidence
672 for an ancient martian ocean in the topography of deformed shorelines, *Nature*,
673 *447*(7146), 840-843.
674 Pieri, D. C. (1980), Martian valleys: Morphology, distribution, age, and origin, *Science*,
675 *210*(4472), 895-897.
676 Roberts, J. H., and S. Zhong (2004), Plume-induced topography and geoid anomalies and their
677 implications for the Tharsis rise on Mars, *Journal of Geophysical Research: Planets*,
678 *109*(E3).
679 Rosenberg, E. N., A. M. Palumbo, J. P. Cassanelli, J. W. Head, and D. K. Weiss (2019), The
680 volume of water required to carve the martian valley networks: Improved constraints
681 using updated methods, *Icarus*, *317*, 379-387.
682 Rossman III, P. I., A. D. Howard, and R. A. Craddock (2008), Fluvial valley networks on Mars,
683 *River confluences, tributaries and the fluvial network*, 419.
684 Rutishauser, A., D. D. Blankenship, M. Sharp, M. L. Skidmore, J. S. Greenbaum, C. Grima, D.
685 M. Schroeder, J. A. Dowdeswell, and D. A. Young (2018), Discovery of a hypersaline
686 subglacial lake complex beneath Devon Ice Cap, Canadian Arctic, *Sci Adv*, *4*(4),
687 eaar4353, doi:10.1126/sciadv.aar4353.

688 Scanlon, K. E., J. W. Head, and D. R. Marchant (2015), Volcanism-induced, local wet-based
689 glacial conditions recorded in the Late Amazonian Arsia Mons tropical mountain glacier
690 deposits, *Icarus*, *250*, 18-31.
691 Schwanghart, W., and N. J. Kuhn (2010), TopoToolbox: A set of Matlab functions for
692 topographic analysis, *Environmental Modelling & Software*, *25*(6), 770-781.
693 Schwanghart, W., and D. Scherler (2014), TopoToolbox 2–MATLAB-based software for
694 topographic analysis and modeling in Earth surface sciences, *Earth Surface Dynamics*,
695 *2*(1), 1-7.
696 Seybold, H. J., E. Kite, and J. W. Kirchner (2018), Branching geometry of valley networks on
697 Mars and Earth and its implications for early Martian climate, *Science advances*, *4*(6),
698 eaar6692.
699 Shreve, R. (1972), Movement of water in glaciers, *Journal of Glaciology*, *11*(62), 205-214.
700 Sommers, A., H. Rajaram, and M. Morlighem (2018), SHAKTI: subglacial hydrology and
701 kinetic, transient interactions v1. 0, *Geoscientific Model Development*, *11*(7), 2955-2974.
702 Sori, M. M., and A. M. Bramson (2019), Water on Mars, with a grain of salt: local heat
703 anomalies are required for basal melting of ice at the South pole today, *Geophysical*
704 *Research Letters*, *46*(3), 1222-1231.
705 Storrar, R. D., C. R. Stokes, and D. J. Evans (2014), Morphometry and pattern of a large sample
706 (> 20,000) of Canadian eskers and implications for subglacial drainage beneath ice
707 sheets, *Quaternary Science Reviews*, *105*, 1-25.
708 Strahler, A. N. (1957), Quantitative analysis of watershed geomorphology, *Eos, Transactions*
709 *American Geophysical Union*, *38*(6), 913-920.
710 Tarboton, D. G. (1997), A new method for the determination of flow directions and upslope
711 areas in grid digital elevation models, *Water resources research*, *33*(2), 309-319.
712 Werder, M. A., I. J. Hewitt, C. G. Schoof, and G. E. Flowers (2013), Modeling channelized and
713 distributed subglacial drainage in two dimensions, *Journal of Geophysical Research:*
714 *Earth Surface*, *118*(4), 2140-2158.
715 Wordsworth, R., F. Forget, E. Millour, J. Head, J.-B. Madeleine, and B. Charnay (2013), Global
716 modelling of the early martian climate under a denser CO2 atmosphere: Water cycle and
717 ice evolution, *Icarus*, *222*(1), 1-19.
718 Wordsworth, R. D. (2016), The climate of early Mars, *Annual Review of Earth and Planetary*
719 *Sciences*, *44*, 381-408.
720 Wordsworth, R. D., L. Kerber, R. T. Pierrehumbert, F. Forget, and J. W. Head (2015),
721 Comparison of "warm and wet" and "cold and icy" scenarios for early Mars in a 3-D
722 climate model, *Journal of Geophysical Research: Planets*, *120*(6), 1201-1219.
723 Yin, A., S. Moon, and M. Day (2021), Landform evolution of Oudemans crater and its bounding
724 plateau plains on Mars: Geomorphological constraints on the Tharsis ice-cap hypothesis,
725 *Icarus*, 114332.
726